Diagnosing evaporative fraction over land from boundary layer clouds

Pierre Gentine

Department of Earth and Environmental Engineering

Columbia University

New York, NY 10027

pg2328@columbia.edu

Craig R. Ferguson

Department of Hydrology and Water Resources Engineering

Institute of Industrial Science

University of Tokyo

Tokyo, Japan

Albert A.M. Holtslag

Meteorology and Air Quality Section

Wageningen University

Wageningen, Netherlands

This article has been accepted for publication and undergone full peer review but has not been through the copyediting, typesetting, pagination and proofreading process, which may lead to differences between this version and the Version of Record. Please cite this article as doi: 10.1002/jgrd.50416

Abstract

The potential use of continental fair-weather shallow cumuli as a way to retrieve the daily surface evaporative fraction over land is evaluated in convective conditions. The proposed method utilizes the fact that both the timing of cloud occurrence and the cloud base height at the time of occurrence provide strong constraints on the surface energy balance and evaporative fraction. The retrieval is especially reliable in the presence of relatively stable and humid free troposphere profiles. The advantage of the method is that it provides a more direct estimate of the surface evaporative fraction than indirect estimation based on inversion of a highly parameterized land surface model. In addition, the evaporative fraction is obtained at a scale of a few kilometers, which is more pertinent for weather and climate studies. The retrieval strategy is tested and validated for three contrasting climates: the U.S. southern Great Plains, West Africa, and the Netherlands. We suggest that the use of satellite observations of shallow cumuli can help constrain the retrieval of the surface evaporative fraction within a data assimilation scheme/reanalysis.

1. Introduction

The potential of near-surface meteorological quantities (i.e., temperature and humidity at screen level) for estimating land surface state was first demonstrated by *Mahfouf* [1991] through the use of a simplified assimilation scheme within a coupled land-atmosphere system. This work was motivated by the realization that the planetary boundary layer (PBL) responds to the surface turbulent heat flux partitioning [e.g., *Brubaker and Entekhabi*, 1995; 1996]. A measure for the latter is the evaporative fraction (EF), the ratio of latent heat flux to the net

available radiation at the land surface, which itself is dependent upon the state of the surface (e.g., surface soil moisture, roughness, leaf area index) [e.g., *Lhomme and Elguero*, 1999; *Gentine et al.*, 2007, *Gentine et al*, 2011a]. The work of *Margulis and Entekhabi* [2003; 2004] went a step further, showing that the PBL and land surface can feedback on one another, and hence, that the assimilation of PBL variables within a coupled land-atmosphere system could yield powerful information about the state of both.

Presently, there is a critical gap in our ability to produce observationally-based estimates of EF, particularly at sub-basin and daily resolutions. The challenges are numerous and the primary limitation is that direct observations, as from the eddy-covariance flux tower measurement network [FLUXNET; *Baldocchi et al.,* 2001], are limited and only locally (10^2-10^3m) representative, although scintillometry allows for measurements over relatively longer path lengths [i.e., several kilometers *De Bruin et al.,* 1995, *Chehbouni et al.,* 1999, *Green et al.,* 2001, *Kohsiek et al.,* 2002, *Hoedjes et al.,* 2007, *Ezzahar et al.,* 2009]. Satellite remote sensing retrievalsavailable as inputs to simplified process models, surface energy balance systems, or other empirical methodologies are limited in temporal coverage by their orbits (generally, sun-synchronous) and in accuracy by the presence of clouds. Atmospheric reanalysis estimates of EF are often unrealistic because the reanalyses do not always assimilate variables that affect (or constrain) EF making the EF very dependent on the details of the land surface model used in the reanalysis. The realism of EF from off-line land surface models, or off-line land reanalyses such as MERRA-Land [*Reichle et al.,* 2011], are limited by the accuracy and consistency of their forcing (i.e., precipitation, radiation, surface pressure, wind, humidity, and air temperature) and of the land-surface models themselves [e.g., *Henderson-Sellers et al.,* 1993; *Boone et al.,* 2009]. Even with *in situ* measurements of this forcing, it is

challenging to calibrate a land surface model to achieve both correct surface energy partitioning and correct infrared temperature [*Gupta et al.,* 1999], a common proxy for water stress and evapotranspiration from remote sensing infrared sensors [*Boulet et al*., 2007].

The dependency of land surface models on screen-level quantities in constraining EF is non-ideal for the following reasons. The use of screen-level quantities necessitates the use of atmospheric stability correction functions because they occur within the atmospheric surface layer [e.g., *Businger et al.*, 1971; *Kader and Yaglom*, 1990; *Beljaars*, 1995; *Katul et al.*, 2011]. These correction functions come with their own uncertainties that impact the accuracy of the retrieved EF. Screen-level is typically below the atmospheric blending height, the height above which measurements sense a statistically homogeneous surface [e.g., *Wieringa*, 1986; *Mason*, 1988; *Garratt*, 1990; *Claussen*, 1995; *Raupach and Finnigan*, 1995]. As such, screen-level variables (particularly, humidity) are prone to substantial temporal variability due to the effects of advection, turbulence, dry-air entrainment (at the PBL top), and variations in land surface temperature [e.g., *Katul et al.*, 1999; *Gentine et al.*, 2011b]. Under most conditions, screen-level variables reflect only the local-scale (hundreds of meters length) inhomogeneities rather than the mean conditions over a larger extent (10^3-10^5m). Unfortunately, it is the broader scale that is of interest for most synoptic weather applications.

In this study, we address the need for a more direct and better-constrained observationally-based estimate of the EF at spatial resolutions relevant to meteorological process studies on a daily time scale. We do so by demonstrating the feasibility of using fair-weather shallow cumuli observations as tracers of the surface energy balance. An important advantage of this method is that cloud cover integrates the surface energy budget response at the horizontal scale of the boundary layer suitable for weather and climate studies [*Wilde and*

Stull; 1985]. In the first part of the manuscript we derive the relationship of the change in relative humidity at the top of the boundary layer as a function of EF and highlight the cloud base and cloud occurrence dependence on EF. The effect of the atmospheric conditions (humidity, stability) on the retrieval capability is then investigated. We finally test our retrieval strategy using three datasets taken from contrasting climates: the 21 June 1997 Atmospheric Radiation Measurement (ARM) Southern Great Plains (SGP) dataset; the 24 June 2006 African Monsoon Multidisciplinary Analysis (AMMA) dataset for Niamey, Niger; and the 31 May 1978 dataset for Cabauw, the Netherlands.

2. Methodology

a. EF and the cumulus-topped boundary layer

EF impacts the state and diurnal development of the convective PBL [*Betts*, 2004], and it appears to be relatively constant under daytime fair-weather conditions [*Crago*, 1996; *Crago and Brutsaert*, 1996; *Lhomme and Elguero*, 1999; *Gentine et al.*, 2007; 2011a]. The influence of EF, or strength of land surface-PBL coupling, is particularly robust in unstable turbulent conditions when the dynamics of the PBL are dominated by surface heating. Strong sensible heating associated with lower EF deepens the PBL and drives the entrainment of dry warm air at the boundary layer top, which in-turn modifies the relative humidity and cloud development at the boundary layer top [*Ek and Holtslag*, 2004; *van Heerwaarden and de Arellano*, 2008, *Westra et al*, 2012, *Gentine et al*, 2013].

The cloud base height reflects the mixed-layer properties, or the equilibrium between surface and synoptic forcing (i.e., radiation and advection) [*Betts and Ball*, 1995; 1998; *Betts*, 2004]. Its height is typically well approximated by the lifting condensation level (LCL) [*Lilly*, 1968; *Betts*, 1973; *Deardorff*, 1979; *Betts*, 2004; *Betts and Viterbo*, 2005; *Betts*, 2007]. The LCL is relatively insensitive to variations across turbulent structures and vertical variations are an order of magnitude smaller than the depth of the entrainment zone on top of the mixed layer [*Wilde et al.*, 1985].

Stull [1985] showed that fair-weather continental cumuli are tracers of thermals born at the bottom of the mixed layer that reach their LCL within the inversion layer. By extension, fair-weather cumuli represent an observable tracer of the inversion layer and PBL height. At their time of occurrence their bases correspond to the top of the PBL [*Wilde et al.*, 1985]. Moister surfaces characterized by higher EF generally induce earlier shallow cumulus development (and larger relative humidity at the PBL top) [*Golaz et al.,* 2001; *Ek and Holtslag*, 2004]. This earlier cloud development is accompanied by a lower PBL through the reduced surface buoyancy flux [*Golaz et al.*, 2001], and hence a lower cloud base. In the next section, we detail how the cloud occurrence time and cloud base may be exploited to retrieve EF.

b. Mixed-layer model and conditions of EF retrieval

The dependence of low-level cloud occurrence on the surface EF is first investigated using a zeroth-order mixed-layer (so called slab) model of the boundary layer under convective conditions with negligible advection [*Lilly*, 1968; *Betts*, 1973; *Deardorff*, 1979]. This simple model allows for the determination of conditions favorable to the development of shallow cumulus as well as the dependency relation between cloud occurrence and LCL on surface and

PBL properties. The model is applied to sample the shallow convection phase occurrence space and to isolate characteristic regimes under which the cloud occurrence will be a reliable estimator of EF. The simple model is able to provide the generality that typical complex models cannot.

Following from several observational studies [*Ek and Mahrt*, 1994; *Chang and Ek*, 1996; *Ek and Holtslag*, 2004], the relative humidity at the mixed layer top can serve as a proxy for cloud occurrence. Specifically, previous studies have shown favorable comparisons of simple slab models with observations under a wide range of conditions. Here we use a 100 percent relative humidity as the indicator of cloud occurrence at the top of the mixed layer, neglecting sub- or super-saturation for simplicity. A more sophisticated cloud cover diagnostic scheme accounting for sub-grid scale variability, such as Bony and Emanuel [2001], could also have been used.

[*Porporato*, 2009] (referred to as P09 hereafter) demonstrated for the case of a linear free-tropospheric profile of potential temperature: $\theta_{\text{free troposphere}}(z) = \theta_{f0} + \gamma_\theta z$, that if we can neglect the early morning transition from the stable to unstable boundary layer, then the mixed layer potential temperature ($\bar{\theta}$) can be approximated by a linear relation to the mixed layer height (z_i):

$$\bar{\theta} = \theta_{f0} + \gamma_\theta' z_i, \qquad (1)$$

where

$$\gamma_\theta' = \frac{1+\beta}{1+2\beta}\gamma_\theta. \qquad (2)$$

Here, θ_{f0} is the free-tropospheric potential temperature profile extended up to the surface, γ_θ is the free-tropospheric potential temperature lapse rate and β is the entrainment efficiency. Both β and γ_θ are assumed constant over the day. We use β=0.2 because it has been shown in literature [e.g., *Lilly*, 1968; *Betts*, 1973; *Deardorff*, 1979] to be a reasonable approximation in the convective boundary layer. Under conditions of strong shear, β increases and this relationship could be included in the model [*Pino*2003]. In this study, we focus on the buoyancy-driven convective boundary layer.

Similarly, P09 showed that the mixed layer specific humidity ($\overline{q}$) could be approximated as a linear function of the mixed layer height if the surface EF is assumed constant (assuming again a linear free-tropospheric profile for specific humidity $q_{\text{free troposphere}}(z) = q_{f_0} + \gamma_q z$):

$$\overline{q} = q_{f0} + \gamma_q{}' z_i, \qquad (3)$$

where q_{f0} is the free-tropospheric specific humidity profile extended up to the surface and

$$\gamma_q{}' = \frac{1}{2}\left(\gamma_\theta \frac{C_p\, EF}{L_v(1+2\beta)(1-EF)} + \gamma_q \right), \qquad (4)$$

and where C_p is the specific heat of dry air, L_v is the latent heat of vaporization of water. The constantEF assumption is supported by several observational studies [e.g., *Crago*, 1996; *Crago and Brutsaert*, 1996; *Lhomme and Elguero*, 1999; *Gentine et al.*, 2007; 2011], at least for daytime fair-sky conditions. The potential temperature lapse rate ($\gamma_\theta{}'$) is always positive (warming) whereas the humidity lapse rate ($\gamma_q{}'$) can be either positive (moistening) or negative (drying).

The relative humidity (RH) tendency at the top of the mixed layer is found using the diagnostic equation of *Ek and Holtslag* [2004] (referred to as EH04 hereafter):

$$\frac{\mathrm{d}RH(z_i)}{\mathrm{d}t} = \frac{R_n - G}{\rho L_v z_i q_s}\left[EF + \mathrm{ne}(1 - EF)\right] \tag{5}$$

where:

$$\mathrm{ne} = \frac{L_v}{C_p}(1+\beta)\left[\frac{\Delta q}{z_i \gamma_\theta} + RH(z_i)\left(\frac{c_2}{\gamma_\theta} - c_1\right)\right], \tag{6}$$

$$c_1 = \frac{L_v}{R_v}\frac{q_s}{T^2}\left(\frac{p}{p_0}\right)^{R_d/C_p}, \tag{7}$$

$$c_2 = \left(\frac{L_v}{R_v}\frac{q_s}{T^2} - \frac{C_p}{R_d}\frac{q_s}{T}\right)\frac{g}{C_p}. \tag{8}$$

R_v and R_d are the gas constants for water vapor and dry air, respectively, ρ is air density, R_n is surface net radiation, G is soil heat flux, g is gravity, T is absolute temperature, q_s is saturation specific humidity at a level just below z_i, Δq is the specific humidity jump above z_i, p is the air pressure at the mixed layer top, p_0 is the surface pressure, ne is the non-evaporative term contributing to the relative humidity tendency, and c_1 and c_2 are coefficients depending on the state of the boundary layer.

Applying Eqn. (3), Δqcan be written:

$$\Delta q = (\gamma_q{}' - \gamma_q) z_i, \tag{9}$$

which can be further simplified from (4) as:

$$\Delta q = \frac{1}{2}\left(\gamma_\theta \frac{C_p}{L_v}\frac{1}{1+2\beta}\frac{EF}{1-EF} - \gamma_q\right) z_i \ . \tag{10}$$

Substituting the above expression for Δq in Eqn. (5) yields:

$$\frac{\mathrm{d}RH(z_i)}{\mathrm{d}t} = \frac{R_n - G}{\rho L_v z_i q_s}\left[\begin{array}{l} EF\left(\dfrac{3+5\beta}{2(1+2\beta)}\right) \\ -\dfrac{L_v\gamma_q}{C_p\gamma_\theta}\dfrac{1+\beta}{2}(1-EF) \\ +(1+\beta)(1-EF)RH(z_i)\dfrac{L_v}{C_p}\left(\dfrac{c_2}{\gamma_\theta}-c_1\right) \end{array}\right]. \qquad (11)$$

We use this equation to investigate the role of EF and free-tropospheric conditions in the development of fair-weather diurnal boundary layer clouds. However, because the RH tendency is related to the diurnal course of available energy at the land surface ($A = R_n - G$) in (11), the precise mechanisms of cloud occurrence may not emerge.

P09 showed that under fair-weather conditions (prior to cloud occurrence) the diurnal cycle of A can be approximated by a parabolic:

$$A(t) = A_0\left[1-\left(\frac{t}{t_0}-1\right)^2\right], \qquad (12)$$

where A_0 the maximum diurnal available energy at the surface, t is in units of hours from sunrise and t_0 is solar noon. This simple parabolic function leads to a clean analytical solution for the boundary layer height by P09, which in our notation reads as:

$$z_i(t) = \left[\frac{2}{3}\frac{(1+2\beta)(1-EF)A_0(3t_0-t)t^2}{\rho C_p\gamma_\theta t_0^2}\right]^{1/2}. \qquad (13)$$

Note that in Eq. (37) of P09 the available energy term is erroneously missing. Eqn. (13) further simplifies the computation of the RH at the mixed layer top. The RH tendency at the PBL top depends on the properties of the boundary layer as highlighted in (11). The state variables themselves (i.e., potential temperature, specific humidity, height) depend on the PBL height

[see equations (1), (10)], which is itself dependent on EF and on the time of day [(13)]. EF therefore constrains the RH at the top of the PBL as a function of time. Consequently, the integration in time of the RH tendency and its value at 100% provides a means to quantify the timing of cloud occurrence as a function of the surface flux partitioning (EF) and free-tropospheric conditions ($\theta_{f0}, q_{f0}, \gamma_\theta, \gamma_q$).

For the purposes of visualization, we apply: (1) the notion that the surface layer RH is often constant when integrated over the course of a day [*Salvucci and Gentine* 2013], and (2) the assumption of a constant lower free-tropospheric relative humidity (hereafter denoted by $\overline{RH}$). Then cloud occurrence may be plotted as a function of EF, the free-tropospheric potential temperature conditions (θ_{f0}, γ_θ), and the lower free-tropospheric relative humidity $\overline{RH}$. Here we will use $A_0 =$ 500 W m^{-2}. In our analyses (not shown), the sensitivity of EF to A_0 was found to be weak.

c. Dependence of cloud base and cloud occurrence on EF

Cloud occurrence and cloud base height are computed as a function of EF, the lower free-tropospheric relative humidity ($\overline{RH}$) and the free-tropospheric potential temperature conditions ($\theta_{f0}, \gamma_\theta$), assuming a linear free-tropospheric profile, $\theta_{\text{free troposphere}}(z) = \theta_{f0} + \gamma_\theta z$. Figure 1 shows that dry atmospheres ($\overline{RH}$=25%) are unlikely to support cloud development at any temperature, except in very weak stratifications, which are rare. At intermediate values of relative humidity ($\overline{RH}$=50%) and warmer temperatures (θ_{f0}=20°C, θ_{f0}=30°C), the time of cloud occurrence delays with increasing EF. In these cases, increased EF reduces entrainment of dry air resulting in a moister (in terms of $\overline{RH}$) boundary layer. Under strong stratifications (

γ_θ>5K/km) and with a cold atmosphere (θ_{f0}=10°C), an opposite behavior is observed: cloud occurrence occurs earlier with increasing EF (Figure 1). In these cases, strong stratification reduces the entrainment of dry free-tropospheric air. The main driver of the boundary layer moistening is then the surface latent heat flux. In a moist atmosphere ($\overline{RH}$=75%), under weak stability (γ_θ<5K/km), the time of cloud occurrence delays with increasing EF (Figure 1). An opposite behavior is observed under strong stability: the time of cloud occurrence is brought forward with increasing EF. The sensitivity of cloud occurrence is especially large at high EF values (EF>0.7). Under these conditions, the timing of cloud occurrence can be a pertinent indicator of EF. Figure 2 shows that in-general cloud base height bears a strong inverse relationship with EF. In all cases the cloud base height is noticeably reduced with increasing EF. Cloud base height is therefore an appropriate tracer of EF in most conditions. From a retrieval perspective, it is worth noticing the change of behavior between strong and weak stability conditions depending on whether dry air entrainment can compensate for surface moistening. Cloud base height (LCL) is always very sensitive to EF. The time of cloud occurrence is an especially pertinent indicator of EF under strong stability (γ_θ>4-5K/km) and high EF values (EF>0.5-0.6).

d. EF retrieval under varying environmental conditions

The accuracy of the EF retrieval using remote sensing products can be evaluated in the context of this simplified mixed-layer model, which models cloud occurrence and cloud base as a function of EF:

$$(\text{Cloud occurence; cloud base}) = f(EF) \qquad (14)$$

In any data assimilation scheme we need to consider both model and measurement errors. In this section, we estimate the retrieval errors assuming a total error in the measurement and modeling of the cloud base height of $\Delta z = 100\text{m}$ and temporal error, Δt, of 30 min. The temporal error corresponds with the resolution offered by the Spinning Enhanced Visible and Infrared Imager [SEVIRI] sensor onboard Meteosat Second Generation geostationary satellites

The retrieval error is computed as the maximum error of the four inverted EF's and is plotted in Figure 3. The inverted EF values are obtained by inversion of the function *f*, in eqn. (14), over the quadrant: (cloud occurrence - $\Delta t/2$, cloud base - $\Delta z/2$); (cloud occurrence - $\Delta t/2$, cloud base + $\Delta z/2$); (cloud occurrence + $\Delta t/2$, cloud base - $\Delta z/2$); (cloud occurrence + $\Delta t/2$, cloud base + $\Delta z/2$).

The disorganization of the solution contours in Figure 3 is due to the nonlinear response of the time of cloud occurrence and cloud base with EF and because the cloud onset is sampled only every Δt. Higher frequency sampling leads to a much smoother contour plot (not shown) but is unrealistic based on temporal resolution currently afforded by satellite-based products. In most conditions the retrieval is relatively accurate with errors below 15%. The retrieval is especially accurate under strong free-tropospheric stability (γ_θ>4.5K/km) and high EF values (EF>0.5) with errors of less than 5% (dark blue). Enhanced retrieval skill in this region of the conditional space could have been expected based on Figures 1 and 2. The retrieval is not performing well in dry conditions (EF<0.4) and with intermediate free-tropospheric stability (3K/km<γ_θ<5K/km), as shown with the red areas in Figure 3. Under these conditions, the cloud base height and time of cloud occurrence is nearly independent of EF as seen in Figures 1 and 2. These conditions are however highly unlikely in reality since the range of values

EF<0.2 corresponds to extremely dry surface conditions (semi-arid or arid), which are generally located in region of strong subsidence with large free-tropospheric stability and therefore with no clouds based on Figure 3. Other than conditions of dry surface and intermediate stability or weak stability and cold atmosphere, the retrieval is accurate to within 5-10%. Reductions in the cloud base height errors to Δz=50m drastically improve the EF retrieval, with maximum errors of about 10% in the driest and least stable atmosphere and accuracies of the order of 2% in the more stable and humid cases (not shown). With a coarser vertical resolution of Δz=200m, the error increases but remains very similar to the case with Δz=100m as seen in Figure 4. The similarity between the two figures highlights the preponderance of the timing of cloud occurrence for the EF retrieval rather the exact cloud base.

3. Case studies

a. Southern Great Plains, U.S. on 21 June 1997

We use the Southern Great Plains (SGP) Atmospheric Radiation Measurement (ARM) observation dataset for 21 June 1997 [*Brown et al.*, 2002] to investigate how the theoretical dependence of shallow cumulus to EF, discussed in the previous section manifests in reality. Golaz et al. [2001] also investigated the dependence to EF for the same case study using a large-eddy simulation and showed strong sensitivity of cloud base and cloud occurrence timing to EF. Figure 5 illustrates the initial atmospheric profiles and imposed surface sensible (H) and latent heat fluxes (λE), as well as their sum (A). The surface heat fluxes are provided at a thirty-minute time step.

A first-order jump model of the convective boundary layer (i.e., a model having a finite inversion layer thickness) is used following the formulation of *vanZanten et al.*[1999] based on *Deardorff* [1979]. The model is depicted in Figure 6. In the control run the model is integrated with prescribed initial sounding and with the observed surface heat fluxes. The model (and first-order models, in-general) is able to accurately reproduce the diurnal course of the convective boundary layer (height, mixed-layer potential temperature and humidity) [*vanZanten et al.*, 1999] despite the fact it is simple and reliant upon a single parameter- the entrainment efficiency at the mixed-layer top β. The model can accurately predict the timing of cloud occurence, which corresponds to the time when the top of the boundary layer (h) (i.e. the top of the inversion) crosses the LCL as seen in Figure 7. In this case study, the mixed-layer state and height are reproduced with less than 4% error (not shown).

In a second set of simulations, EF is assumed constant during daytime and is varied from 0.1 to 0.95 to investigate the effect of a change in the surface heat flux partitioning on the timing of cloud occurrence. The diurnal course of available energy, $A(t)$, is assumed fixed across all simulations. In practice, $A(t)$ can be obtained as output from a land surface model, from in-situ measurements, or from satellite remote sensing. For instance, if soil heat flux (G) can be estimated, then observations of net radiation (R_n) from satellite remote sensing could be used to estimate A as R_n minus G. Figure 8 depicts the time of cloud occurrence and coincident cloud base (LCL) at the temporal resolution of the model (30 minutes) obtained with the different EF runs. It shows that cloud occurrence is delayed with increasing EF. For higher EF's, the reduced growth rate of the boundary layer cannot compensate for the LCL reduction, which explains the delayed cloud occurrence. The zeroth-order model (section 2.d)

also captured this dependency. For a given time of cloud occurrence, the LCLdecreases with EF, corresponding to a shallower and moister boundary layer. This phenomenon is especially apparent for high values of EF.

Two sensitivity experiments are carried out to assess the impact of the vertical stability and humidity on the retrieval. In the first, an increase in the potential temperature gradient of 1K km^{-1} was imposed. In the second, the initial specific humidity profile was increased by 1g kg^{-1}. The modified profiles are illustrated in Figures 5b and c. A greater moisture lapse rate in the free troposphere increases the specific humidity of the mixed layer as evident in equations (3) and (4). Figure 8 shows that with increased stability the LCL estimates are more sensitive to the exact value of EF. This matches result from the zero-th order model (Figures 1 and 2). Warm air entrainment into the mixed layer drastically impacts the saturation specific humidity through the Clausius-Clapeyron relationship. The LCL is thus more controlled by EF with increased stability. In other words, with increased stability the estimation of EF becomes more accurate. Conversely, an increase in the initial profile humidity does not substantially impact the retrievability of EF. The entrained air is moister, but the boundary layer height is only marginally affected because buoyancy is largely driven by the temperature gradient. As a consequence, at high values of EF (EF>0.6), the LCLis lowered due to the concentration of moist air in the shallow boundary layer [*EH04*; as also seen in Figure 2]. Overall the results from this case support the model's applicability for humid conditions (EF>0.6) or under strong free-tropospheric stratifications.

b. Niamey, Niger on 24 June 2006

For our second case study, we use data from the African Monsoon Multidisciplinary Analysis [AMMA; Redelsperger et al. 2006] measurement campaign in the semiarid Sahel. We focus on June 24 2006, a day with shallow cumulus development. The early morning radiosonde profiles were obtained from the AMMA site of Niamey international Airport (13.477°N, 2.175°E, 225m above sea level). We use surface turbulent heat flux measurements from an eddy-covariance system located at the ARM mobile facility setup just outside Niamey airport. The reader is referred to *Westra et al*. [2012] for more details on the dataset.

Figure 9 depicts the atmospheric profile obtained using radisoundings at 0834UTC, 1135UTC, 1432UTC and 1732UTC on June 24, 2006. On that day, the 2m air temperature reached 40°C. The early-morning lapse rate of potential temperature between 1000 and 3000m was 2.95K/km and the mixed layer reached 1700m at 1731UTC and a layer of shallow cumulus clouds developed between 1030 and 1100LT, that is between 1130 and 1200UTC. The cloud base height information was not available, but with this added information we would expect the retrieval of EF to improve. The mean daylight EF was 0.12 with a minimum of about 0.08 at 1400UTC based on the eddy-covariance measurements. Observed weather station measurements revealed a southerly wind in the lower layer advecting moist air with 0.3g kg^{-1} hr^{-1} [*Westra et al*. 2012].

We ran the first-order PBL model for different daytime EF values ranging from 0.1 to 0.8 in increments of 0.1, using the smoothed profile described in Figure 9 (dashed line). The results are depicted in Figure 10. As could be expected (Figure 1) increased EF leads to lower and colder PBL (in terms of potential temperature). The mixed-layer specific humidity

increases with EF yet the relative humidity decreases with EF, as pointed out by *EH04*, *Westra et al.* [2012], *Huang and Margulis* [2012] and *Gentine et al.* [2013] under weak stratification and over dry surfaces. Moister surfaces (higher EF) have lower relative humidity at the boundary layer top.

The timing of cloud occurrence can easily be diagnosed as the crossover time of the 100% relative humidity level of the boundary layer top (i.e. height h of the bulk model) and is depicted in Figure 11 as a function of EF with 0.025 increments in EF. The time of cloud occurrence increase with EF under this weak stratification case points to a dry case soil advantage for cumulus occurrence [*Westra et al.* 2012, *Gentine et al.* 2013], as observed with the simple model in Figure 1. The cloud base height at the time of occurrence decreases with EF since the boundary layer height is reduced with increasing EF, in accordance with the results of Figure 2 obtained with the simplified model. Both the time of cloud occurrence and the cloud base are monotonic with EF. The retrieval of EF is thus facilitated by this nearly monotonic relationship with EF. Using the cloud onset time information, Figure 11a, we would estimate a daytime EF value ranging between 0.05 and 0.1. This estimated value is close to the observed values of the mean diurnal EF, 0.12 and minimum EF, 0.08. This provides further validation for the utility of our new EF estimation methodology.

c. Cabauw, the Netherlands on 31 May 1978

To illustrate the onset of boundary-layer clouds in more humid and colder conditions, athird contrasting dataset is used for Cabauw, the Netherlands. The data were observed on the morning of May 31, 1978. The reader is referred to *Holtslag et al*. [1995] and EH04 for details on the observations. The profiles at 6AM are shown in Figure 12. Sensible and latent heat

fluxes were determined from Bowen ratio methods at the Cabauw site. The daytime EF was 0.77 and the diurnal minimum was 0.72 based on the surface Bowen ration measurements. The 2m air temperature reached 26°C at 1600UTC and the 2m specific humidity was fairly constant between 7 to 8g/kg during the course of the day. A fair-weather cumulus cloud layer developed between 1430 and 1500UTC, as evidenced by the diurnal course of net radiation in Figure 12 and further described in EH04. The free-tropospheric potential temperature lapse rate was 3.7 K/km and the specific humidity lapse rate was -1.6 g/kg/km.

Our bulk model is initialized with the 6AM sounding (similarly to EH04) and is run with a 30-minute resolution forcing. As in the AMMA case, the EF is varied with 0.025 increments in order to diagnose the timing of cloud occurrence, which is depicted in Figure 13. With a 30-min resolution output the diagnosed EF corresponding to the shallow cumulus occurrence timing (1430 to 1500UTC) would be in the range 0.625 to 0.75, which is close to the observed mean and minimum daily data, 0.77 and 0.72 respectively. Higher observing and model output resolution would refine the EF retrieval. This further confirms the model representativeness for relatively cold and humid summer conditions.

3. Conclusions

We have demonstrated that under many climatic conditions, observations of fair-weather shallow cumuli permit a relatively accurate estimation of the evaporative fraction, - a feature that remains a major stumbling block for land surface modeling and meteorological forecasting. In unstable turbulent conditions, observations of the timing of cloud occurrence and cloud base height provide fundamental and very useful information about the surface turbulent heat flux partitioning.

The advantages of a cloud field-based approach are that it applies to scales directly relevant to weather or climate studies through horizontal aggregation by the boundary layer blending and it can rely on very limited assumptions about the surface and boundary layer state, because on principles of heat and moisture conservation within the boundary layer. Importantly, the methodology provides an estimate of the surface energy balance partitioning under partly cloudy cases.

The retrieval methodology is tested on representative case days from three diverse climate regimes over the ARM SGP, AMMA and Cabauw sites. In all cases the retrieved evaporative fraction compares favorably against observations, suggesting the potential for general applicability of the method.

Based on our findings, we suggest that assimilating cloud cover and cloud base height (LCL) information into a coupled land-boundary layer scheme could improve the retrieval of the surface heat flux partitioning, especially in humid environments, with relatively stable/stratified conditions above the boundary layer. An immediate application of this method is towards improved representation of the boundary layer heat budget in atmospheric reanalysis products [*Steeneveld et al,* 2011]. Currently, satellite-based cloud observations are available to facilitate these EF retrievals- in many cases since 1979. Planned observing systems, such as the GOES-R Series (http://www.goes-r.gov) scheduled for launch in 2015, will serve to further enhance the potential skill of EF retrievals over land from clouds through improved measurement accuracy and spatio-temporal resolution. Global maps of land-atmosphere interaction strength [e.g., *Ferguson et al.,* 2012; *Dirmeyer et al*., 2012] provide an approximate spatial extent of the area where cloud field-based EF estimates stand to provide the greatest additional information. This work will be explored in a forthcoming publication.

Acknowledgments

We thank Michael Ek (NCEP), Gert-Jan Steeneveld (Wageningen University), Françcoiseguichard (Météo France) for providing their selections of the Cabauw and AMMA data sets, respectively. Craig Ferguson was supported by Japan Society for the Promotion of Science Postdoctoral Fellowship for Foreign Researchers P10379: Climate change and the potential acceleration of the hydrological cycle. Pierre Gentine was supported by grant NSF-AGS 1035843: Collaborative Research: Quantifying the impacts of atmospheric and land surface heterogeneity and scale on soil moisture-precipitation feedbacks.

References

Baldocchi, D., Falge, E., Gu, L., Olson, R., Hollinger, D., Running, S., Anthoni, P., et al. (2001). FLUXNET: A new tool to study the temporal and spatial variability of ecosystem-scale carbon dioxide, water vapor, and energy flux densities. *B Am MeteorolSoc*, *82*(11), 2415–2434.

Beljaars, A. (1995), The Parametrization of Surface Fluxes in Large-Scale Models Under Free-Convection, *Q J Roy Meteor Soc*, *121*(522), 255–270.

Betts, A. (1973), Non-precipitating cumulus convection and its parameterization, *Q J Roy Meteor Soc*, *99*(419), 178–196.

Betts, A. (2004), Understanding hydrometeorology using global models, *B Am Meteorol Soc*, *85*(11), 1673, doi:10.1175/BAMS-85-11-1673.

Betts, A. K. (2007), Coupling of water vapor convergence, clouds, precipitation, and land-surface processes, *J Geophys Res-Atmos*, *112*(D10), D10108, doi:10.1029/2006JD008191.

Betts, A. K., and J. Ball (1995), The FIFE surface diurnal cycle climate, *J Geophys Res-Atmos*, *100*, 25679–25693.

Betts, A. K., and J. Ball (1998), FIFE surface climate and site-average dataset 1987-89, *J Atmos Sci,* 55, 1091–1108.

Betts, A., and P. Viterbo (2005), Land-surface, boundary layer, and cloud-field coupling over the southwestern Amazon in ERA-40, *J Geophys Res-Atmos*, *110*(D14), D14108–, doi:10.1029/2004JD005702.

Bony, S., and K. Emanuel (2001), A parameterization of the cloudiness associated with cumulus convection; Evaluation using TOGA COARE data, *J Atmos Sci*, *58*(21), 3158–3183.

Boone, A. et al. (2009), The AMMA Land Surface Model Intercomparison Project (ALMIP), *B Am Meteorol Soc*, *90*(12), 1865–1880, doi:10.1175/2009bams2786.1.

Brown, A. et al. (2002), Large-eddy simulation of the diurnal cycle of shallow cumulus convection overland, *Q J Roy Meteor Soc*, *128*(582), 1075–1093.

Brubaker, K. L., and D. Entekhabi (1996), Analysis of feedback mechanisms in land-atmosphere interaction, *Water resources Research*, *32*(5), 1343–1357.

Brubaker, K., and D. Entekhabi (1995), An analytic approach to modeling land atmosphere interaction 1. Construct and equilibrium behavior, *Water resources Research*, *31*(3), 619–632.

Businger, J., J. Wyngaard, Y. Izumi, and E. Bradley (1971), Flux-Profile Relationships in Atmospheric Surface Layer, *J Atmos Sci*, *28*(2), 181–&.

Chang, S., and M. Ek (1996), Daytime evolution of relative humidity at the boundary layer top, *Mon Weather Rev*, *124*(6), 1323–1326.

Chehbouni, A., C. Watts, J. Lagouarde, Y. Kerr, J. Rodriguez, J. Bonnefond, F. Santiago, G. Dedieu, D. Goodrich, and C. Unkrich (2000), Estimation of heat and momentum fluxes over complex terrain using a large aperture scintillometer, *Agr Forest Meteorol*, *105*(1-3), 215–226.

Claussen, M. (1995), Flux Aggregation at Large Scales - on the Limits of Validity of the Concept of Blending Height, *J Hydrol*, 166, 371–382.

Crago, R. (1996), Conservation and variability of the evaporative fraction during the daytime, *J Hydrol*, *180*(1-4), 173–194.

Crago, R., and W. Brutsaert (1996), Daytime evaporation and the self-preservation of the evaporative fraction and the Bowen ratio, *J Hydrol*, *178*(1-4), 241–255.

DeBruin, H., B. vandenHurk, and W. Kohsiek (1995), The scintillation method tested over a dry vineyard area, *Bound-Lay Meteorol*, *76*, 25–40.

Deardorff, J. W. (1979), Prediction of convective mixed-layer entrainment for realistic capping inversion structure, *J Atmos Sci*, *36*(3), 424–436.

Dirmeyer, P. A., B. A. Cash, and J. L. Kinter III (2012), Evidence for enhanced land-atmosphere feedback in a warming climate, *J Hydrometeorol*, *13*, 981–995.

Ek, M. B., and A. Holtslag (2004), Influence of soil moisture on boundary layer cloud development, *J Hydrometeorol*, *5*(1), 86–99.

Ek, M., and L. Mahrt (1994), Daytime Evolution of Relative-Humidity at the Boundary-Layer Top, *Mon Weather Rev*, *122*(12), 2709–2721.

Ezzahar, J., A. Chehbouni, J. Hoedjes, D. Ramier, N. Boulain, S. Boubkraoui, B. Cappelaere, L. Descroix, B. Mougenot, and F. Timouk (2009), Combining scintillometer measurements and an aggregation scheme to estimate area-averaged latent heat flux during the AMMA experiment, *J Hydrol*, *375*, 217–226, doi:10.1016/j.jhydrol.2009.01.010.

Ferguson, C. R., E. F. Wood, and R. K. Vinukollu (2012), A Global Intercomparison of Modeled and Observed Land-Atmosphere Coupling, *J Hydrometeorol*, *13*(3), 749-784.

Garratt, J. (1990), The internal boundary layer—A review, *Bound-Lay Meteorol*.

Gentine, P., D. Entekhabi, A. Chehbouni, G. Boulet, and B. Duchemin (2007), Analysis of evaporative fraction diurnal behaviour, *Agr Forest Meteorol*, *143*, 13–29, doi:10.1016/j.agrformet.2006.11.002.

Gentine, P., D. Entekhabi, and J. Polcher (2011a), The Diurnal Behavior of Evaporative

Fraction in the Soil-Vegetation-Atmospheric Boundary Layer Continuum, *J Hydrometeorol*, *12*(6), 1530–1546, doi:10.1175/2011JHM1261.1.

Gentine, P., J. Polcher, and D. Entekhabi (2011b), Harmonic propagation of variability in surface energy balance within a coupled soil-vegetation-atmosphere system, *Water resources Research*, *47*, –, doi:10.1029/2010WR009268.

Gentine, P., A. A. M. Holtslag, F. D'Andrea, and M. Ek (2013), Surface and atmospheric controls on the onset of moist convection over land, *J Hydrometeorol*, 130211131121003, doi:10.1175/JHM-D-12-0137.1.

Golaz, J.-C., H. Jiang, and W. R. Cotton (2001), A large-eddy simulation study of cumulus clouds over land and sensitivity to soil moisture, *Atmos Res*, *59-60*, 373–392, doi:10.1016/S0169-8095(01)00113-2.

Green, A., M. Astill, K. McAneney, and J. Nieveen (2001), Path-averaged surface fluxes determined from infrared and microwave scintillometers, *Agr Forest Meteorol*, *109*(3), 233–247.

Henderson-Sellers, A., Z. L. Yang, and R. E. Dickinson (1993), The Project for Intercomparison of Land-surface Parameterization Schemes, *B Am Meteorol Soc*, *74:7*.

Hoedjes, J. C. B., A. Chehbouni, J. Ezzahar, R. Escadafal, and H. A. R. De Bruin (2007), Comparison of large aperture scintillometer and eddy covariance measurements: Can thermal infrared data be used to capture footprint-induced differences? *J Hydrometeorol*, *8*(2), 144–159, doi:10.1175/JHM561.1.

Holtslag, A.A.M., E. van Meijgaard, and W.C. de Rooy, 1995: A comparison of boundary-layer diffusion schemes in unstable conditions over land. *Boundary-Layer Meteorol.*, 76, 69 - 95.

Huang, H.-Y., & Margulis, S. A. (2011). Investigating the Impact of Soil Moisture and Atmospheric Stability on Cloud Development and Distribution Using a Coupled Large-Eddy Simulation and Land Surface Model. *J Hydrometeorol*, *12*(5), 787–804. doi:10.1175/2011JHM1315.1

Kader, B., and A. Yaglom (1990), Mean Fields and Fluctuation Moments in Unstably Stratified Turbulent Boundary-Layers, *Journal of Fluid Mechanics*, *212*, 637–662.

Katul, G. et al. (1999), Spatial variability of turbulent fluxes in the roughness sublayer of an even-aged pine forest, *Bound-Lay Meteorol*, *93*(1), 1–28.

Katul, G. G., A. G. Konings, and A. Porporato (2011), Mean Velocity Profile in a Sheared and Thermally Stratified Atmospheric Boundary Layer, *Phys Rev Lett*, *107*(26), –, doi:10.1103/PhysRevLett.107.268502.

Kohsiek, W., W. Meijninger, A. Moene, B. Heusinkveld, O. Hartogensis, W. Hillen, and H. De Bruin (2002), An extra large aperture scintillometer for long range applications, *Bound-Lay Meteorol*, *105*(1), 119–127.

Lhomme, J., and E. Elguero (1999), Examination of evaporative fraction diurnal behaviour using a soil-vegetation model coupled with a mixed-layer model, *Hydrol Earth Syst Sc*, *3*(2), 259–270.

Lilly, D. K. (1968), Models of Cloud-Topped Mixed Layers Under a Strong Inversion, *Q J Roy Meteor Soc*, *94*(401), 292–&.

Mahfouf, J. F. (1991), Analysis of soil moisture from near-surface parameters - A feasibility study, *J Appl Meteorol*, *30*(11), 1534–1547.

Margulis, S. A., and D. Entekhabi (2003), Variational assimilation of radiometric surface temperature and reference-level micrometeorology into a model of the atmospheric boundary layer and land surface, *Mon Weather Rev*, *131*(7), 1272–1288.

Margulis, S. A., and D. Entekhabi (2004), Boundary-layer entrainment estimation through assimilation of radiosonde and micrometeorological data into a mixed-layer model, *Bound-Lay Meteorol*, *110*(3), 405–433.

Mason, P. (1988), The formation of areally-averaged roughness lengths, *Q J Roy Meteor Soc*, *114*(480), 399–420.

Pino, D., J. Vilà-Guerau de Arellano, and P. Duynkerke (2003), The contribution of shear to the evolution of a convective boundary layer, *J Atmos Sci*, *60*(16), 1913–1926.

Porporato, A. (2009), Atmospheric Boundary-Layer Dynamics with Constant Bowen Ratio, *Bound-Lay Meteorol*, *132*(2), 227–240, doi:10.1007/s10546-009-9400-8.

Raupach, M., and J. Finnigan (1995), Scale issues in boundary-layer meteorology: surface energy balances in heterogeneous terrain, *Hydrol Process*.

Redelsperger, J.-L., Thorncroft, C. D., Diedhiou, A., Lebel, T., Parker, D. J., & Polcher, J. (2006). African monsoon multidisciplinary analysis - An international research project and field campaign. *B Am Meteorol Soc y*, *87*(12), doi:10.1175/BAMS-87-12-1739

Reichle, R. H., R. D. Koster, and G. De Lannoy (2011), Assessment and Enhancement of MERRA Land Surface Hydrology Estimates, *J Climate*, *24*, 6322–6334.

Salvucci G. and P. Gentine (2013) , Variability of Relative Humidity Reveals and Estimate Land Surface Controls on Evapotranspiration, *PNAS*, doi: 10.1073/pnas.1215844110.

van Heerwaarden, C. C., and J. V.-G. de Arellano (2008), Relative humidity as an indicator for cloud formation over heterogeneous land surfaces, *J Atmos Sci*, *65*(10), 3263–3277, doi:10.1175/2008JAS2591.1.

vanZanten, M. C., P. Duynkerke, and J. Cuijpers (1999), Entrainment parameterization in convective boundary layers, *J Atmos Sci*, *56*(6), 813–828.

Westra, D., Steeneveld, G. J., & Holtslag, A. A. M. (2012). Some Observational Evidence for Dry Soils Supporting Enhanced High Relative Humidity at the Convective Boundary Layer Top. *J Hydrometeorol*, 1347–1358.

Wieringa, J. (1986), Roughness-Dependent Geographical Interpolation of Surface Wind-Speed Averages, *Q J Roy Meteor Soc*, *112*(473), 867–889.

Wilde, N., R. Stull, and E. Eloranta (1985), The Lcl Zone and Cumulus Onset, *J Clim Appl Meteorol*, *24*(7), 640–657.

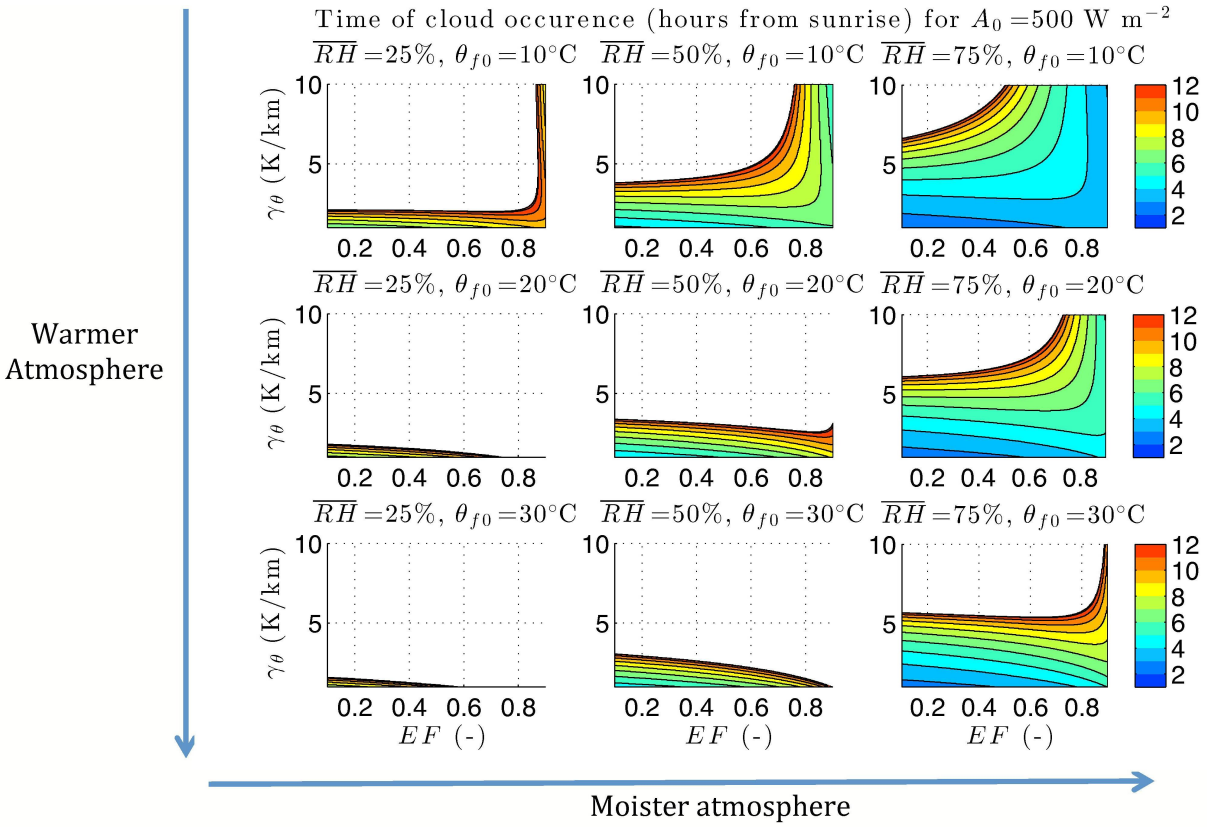

Figure 1:Time of cloud occurrence in hours from sunrise as a function of EF for a maximum available energy A_0 = 500 W m^{-2} and for varying values of free-tropospheric humidity and free-tropospheric surface potential temperature. The free troposphere is more humid to the right and warmer to the bottom.

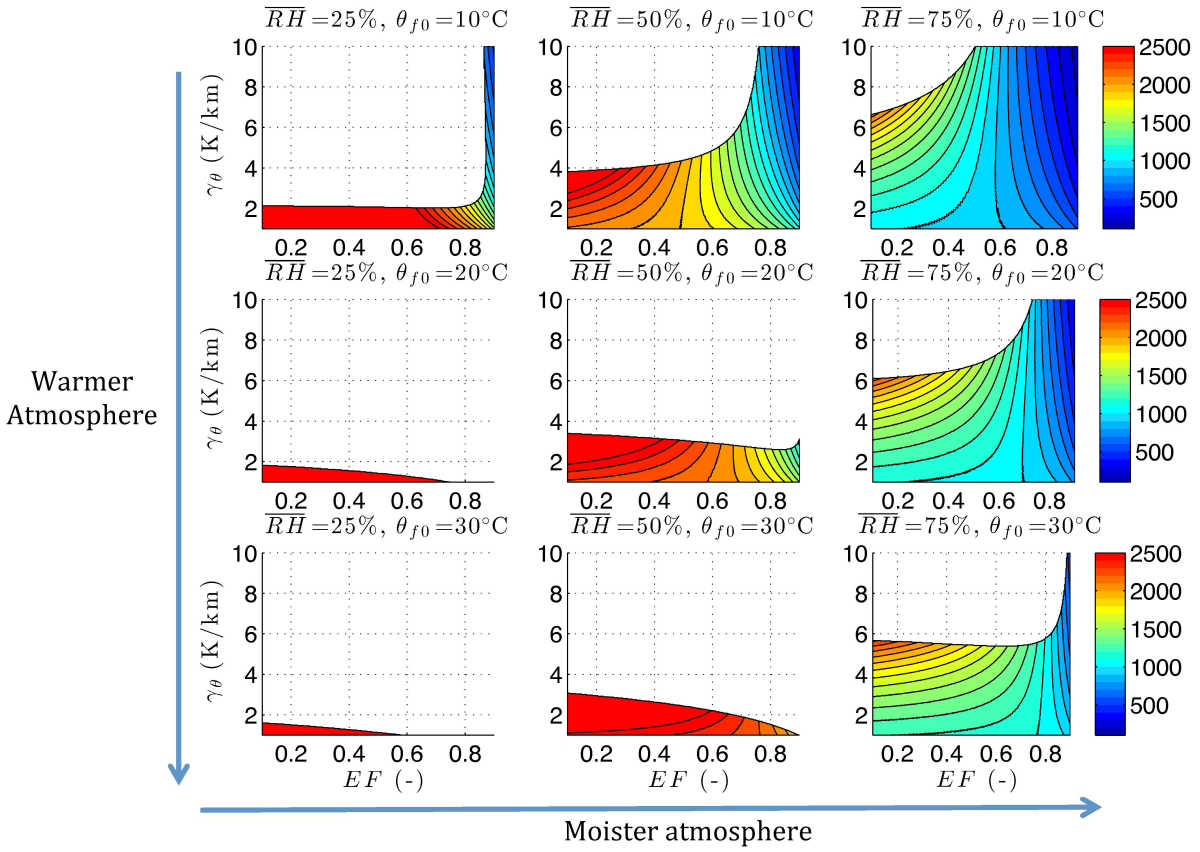

Figure 2:Cloud base (LCL) height in meters at the time of cloud occurrence as a function of evaporative fraction for a maximum available energy A_0 = 500 W m^{-2} and for varying values of free-tropospheric humidity and free-tropospheric surface potential temperature. The free troposphere is more humid to the right and warmer to the bottom.

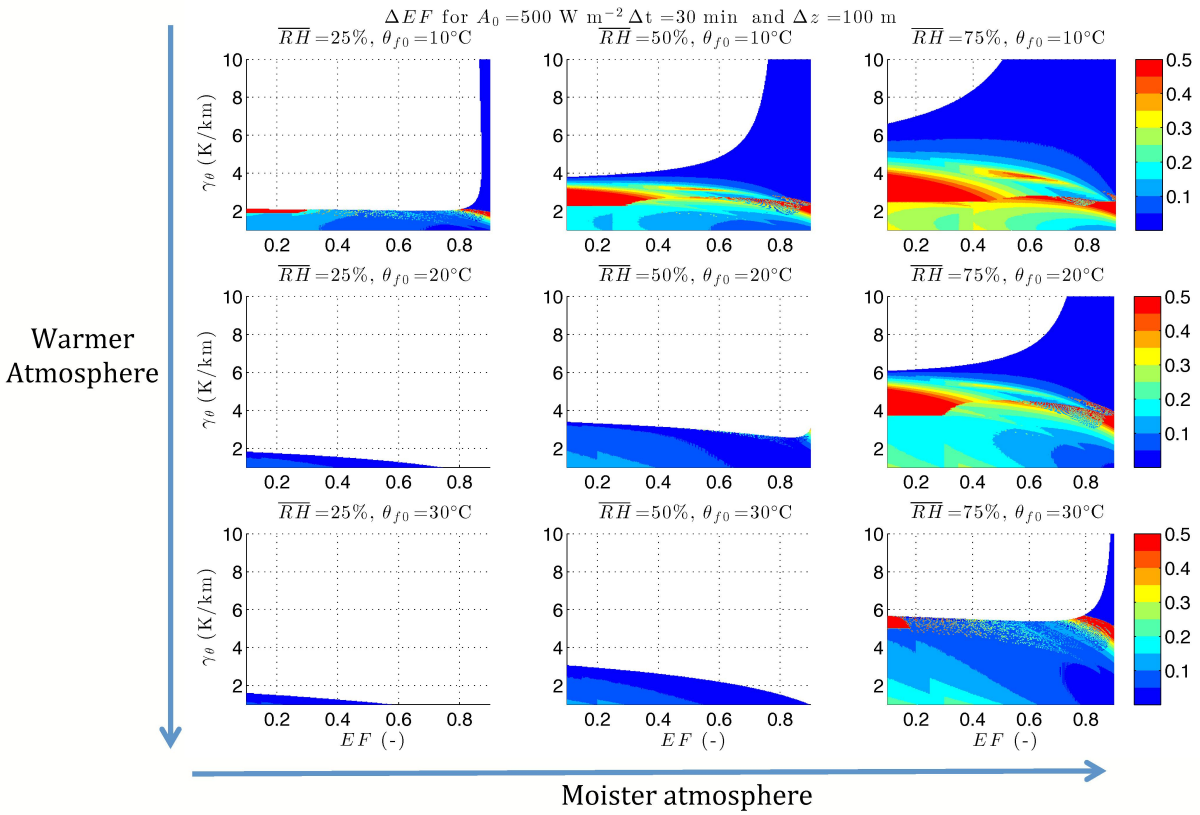

Figure 3:Error in EF retrieval, ΔEF, for varying values of free-tropospheric humidity and free-tropospheric surface potential temperature. The free troposphere is more humid to the right and warmer to the bottom. The error in the timing of cloud occurrence is assumed to be $\Delta t = 30\,\mathrm{min}$ and the error in the cloud base height is $\Delta z = 100\,\mathrm{m}$.

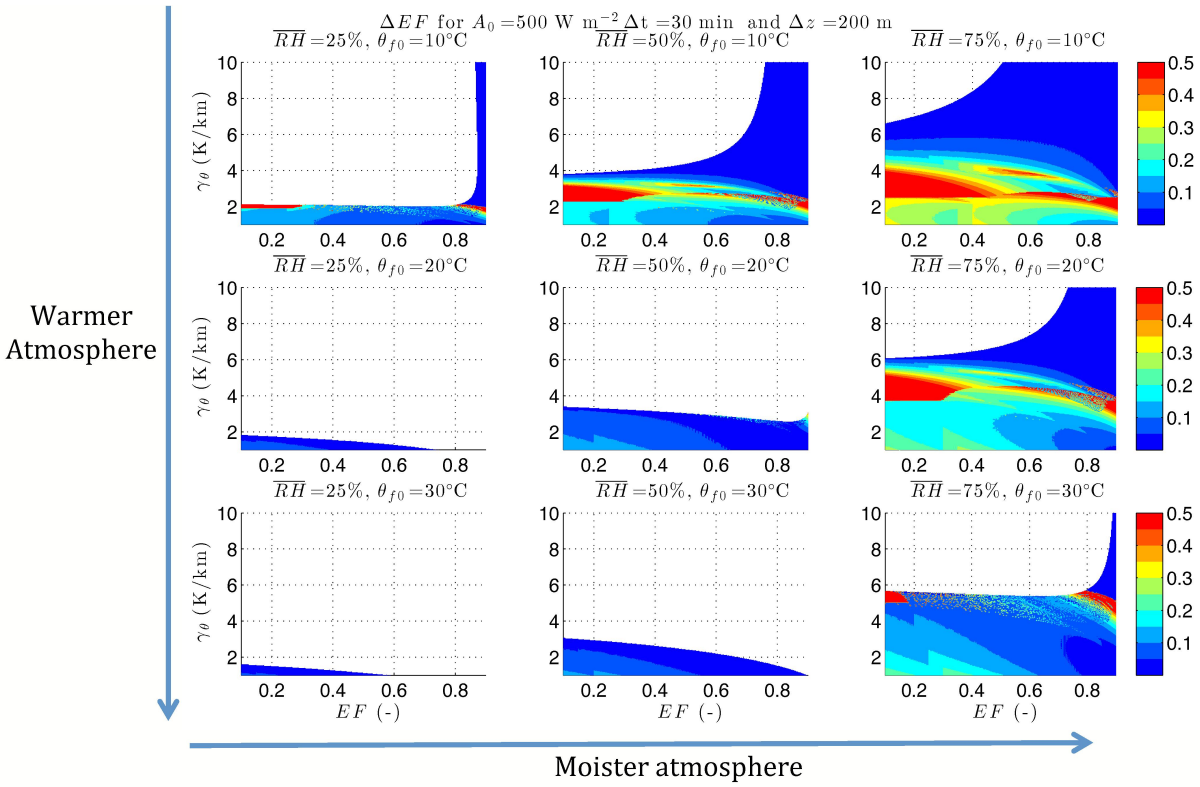

Figure 4: Same as Figure 3 but with $\Delta z = 200\text{m}$.

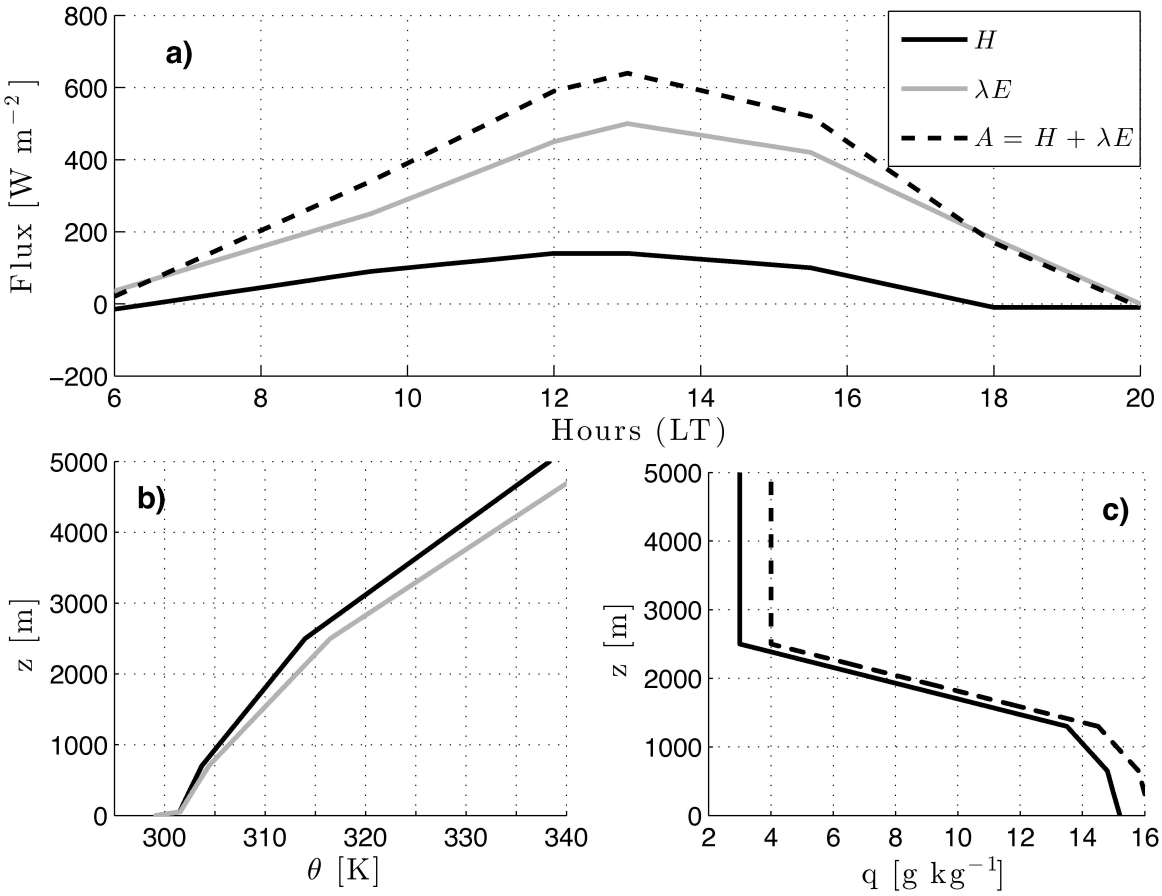

Figure 5: a) Forcing of sensible heat flux (H), latent heat flux (λE) and their sum, the available energy (A) for the ARM SGP testcase. b) Potential temperature initial profile (black) and perturbed profile (gray) with 1Kkm^{-1} increased stability. c) Specific humidity initial profile (black) and perturbed profile (dashed line).

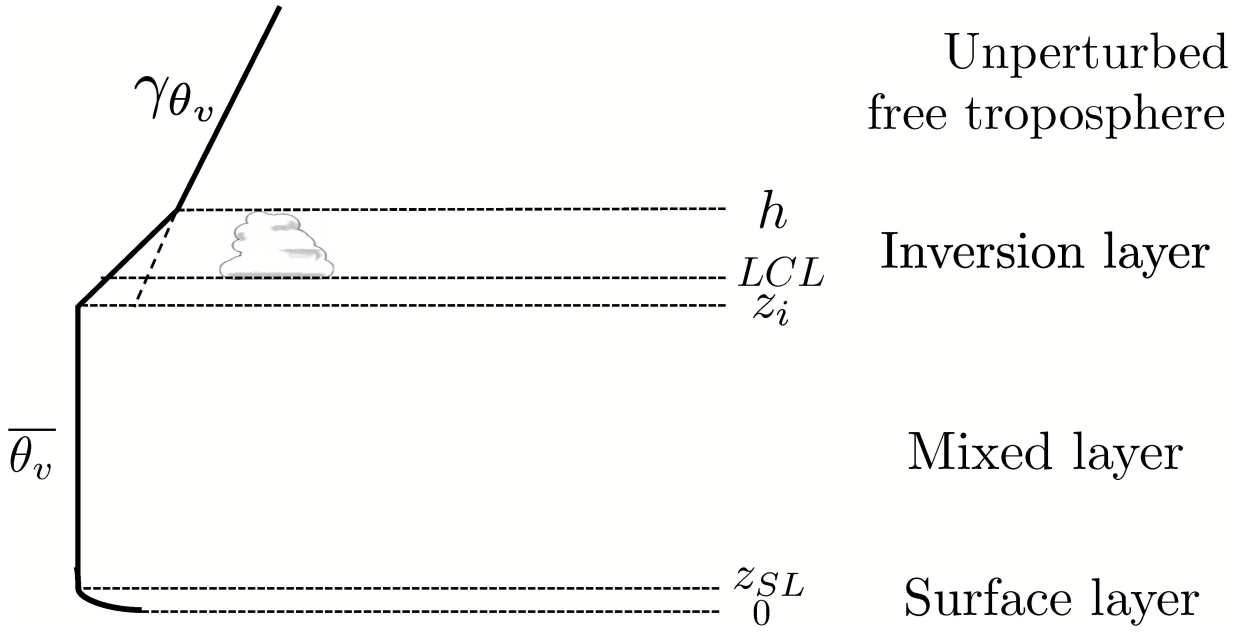

Figure 6: Profile of the virtual potential temperature θ_v in the first-order boundary layer model.z_{sl} is the top of the surface layer, z_i the top of the mixed layer, *LCL* is the lifting condensation level, *h* is the top of the boundary layer.

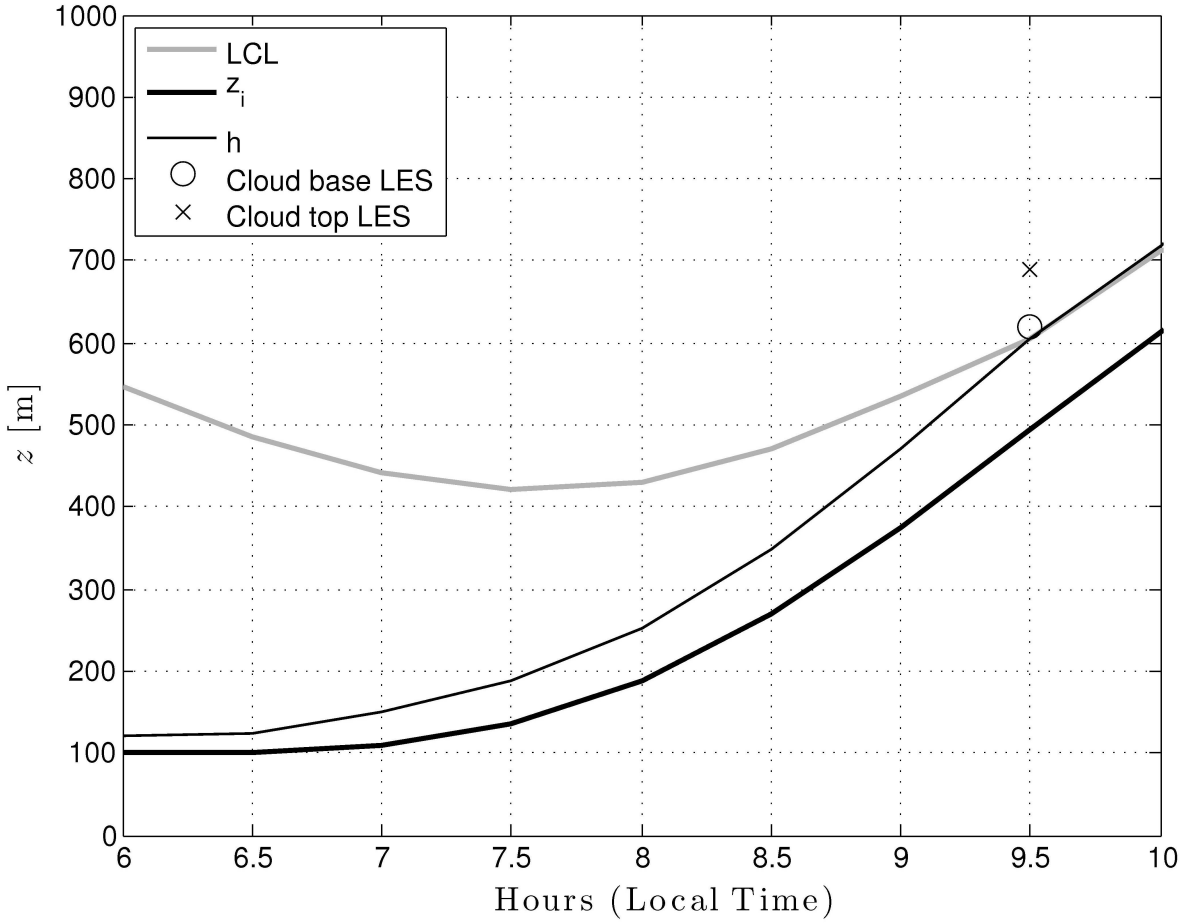

Figure 7: Mixed-layer height z_i, top of the inversion h and Lifting Condensation Level (LCL) of the first-order boundary layer model compared to the cloud base height diagnosed as the mean of 8 large-eddy simulation models **[*Brown et al.*, 2002]** for the ARM SGP dataset. The cloud top at time of occurrence is depicted as an indication of the vertical extent of the shallow cumuli.

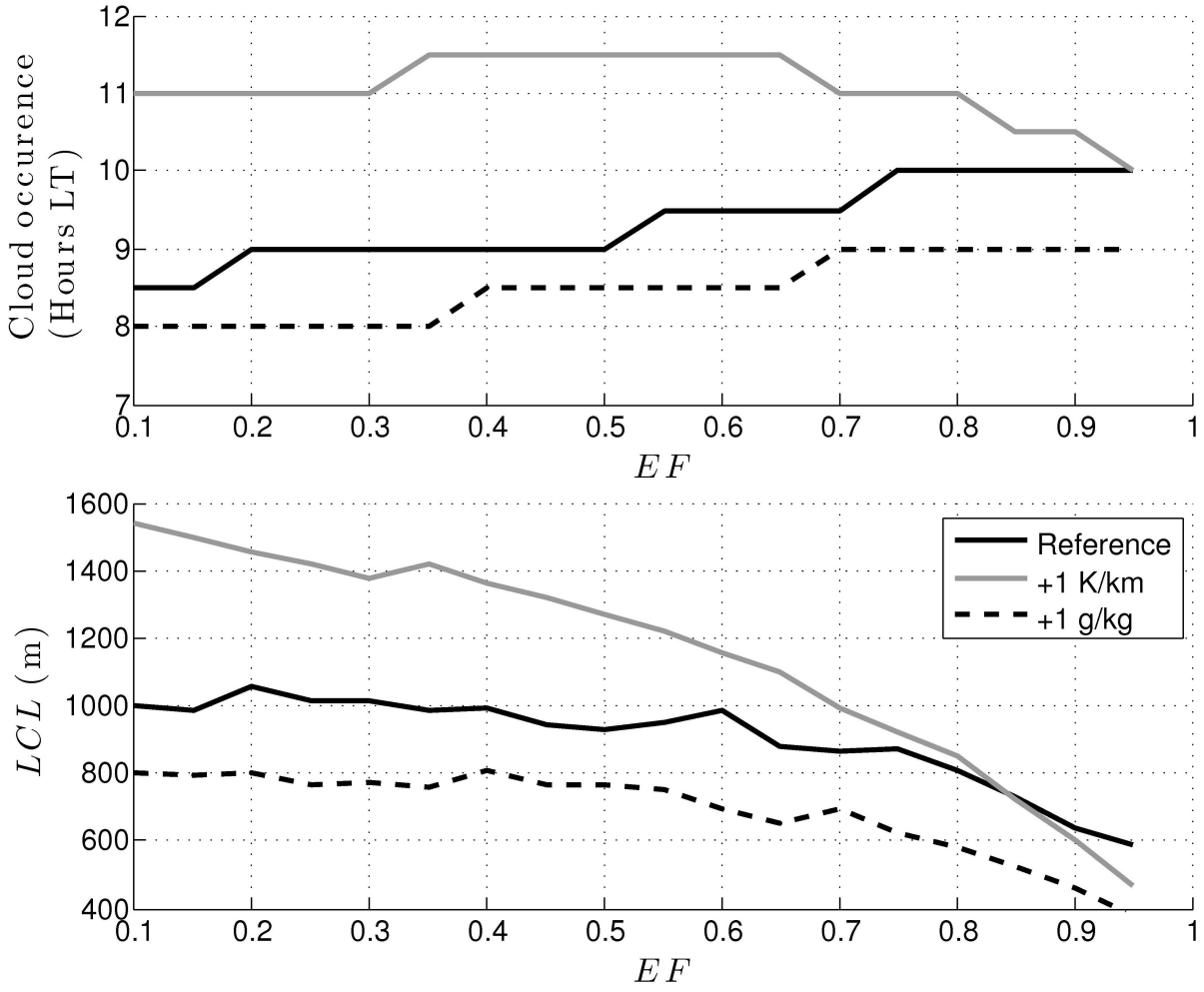

Figure 8: (top) Local time of cloud occurrence (with resolution of 30-minutes) and (bottom) Lifting Condensation Level (*LCL*) at the time of occurrence, as a function of Evaporative Fraction (*EF*) for the ARM SGP dataset. The solid black line corresponds with the reference profile shown in Figure 5(b- c). The solid gray line corresponds with the enhanced atmospheric stability case (i.e., potential temperature increased by 1K km^{-1}). The dashed black line corresponds with enhanced humidity case (i.e., specific humidity increased by 1 g kg^{-1}).

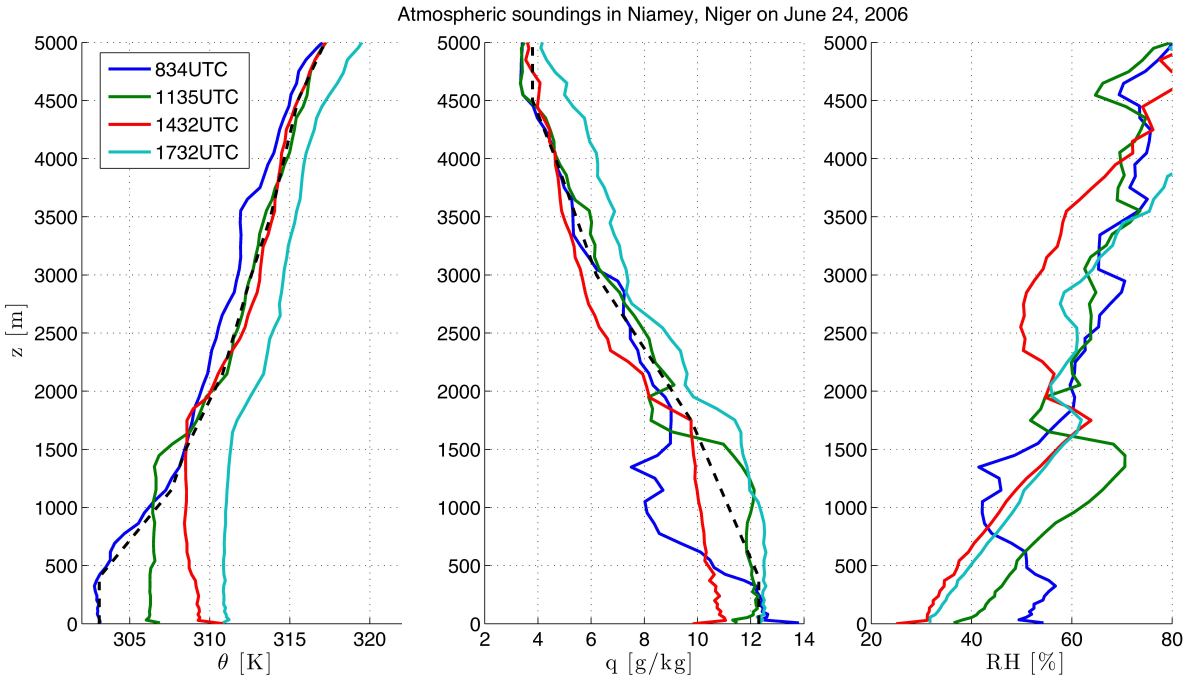

Figure 9: Profiles of potential temperature (left), specific humidity (middle) and relative humidity (right) obtained by radiosounding launched at 8.34UTC, 1135UTC, 1431UTC, 1731UTC, June 24, 2006 for the AMMA dataset in Niamey, Niger. Dashed line represents the smoothed profile used to initialize the runs.

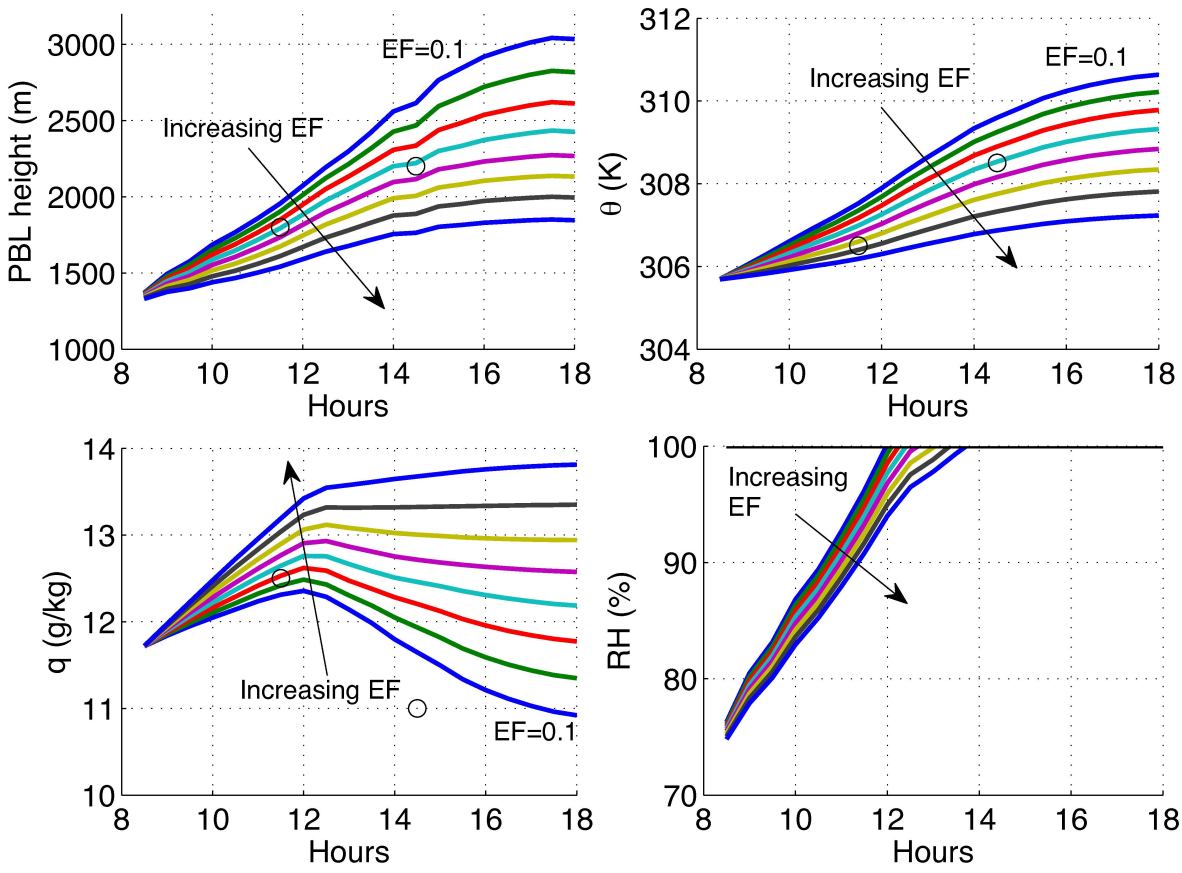

Figure 10: Diurnal evolution of the PBL height, potential temperature, specific humidity in the mixed layer and the relative humidity at the mixed layer top over the AMMA test case for EF varying between 0.1 and 0.8 with 0.1 increment. The relative humidity is not constrained to go below a hundred percent to facilitate the diagnostic of the crossover of the relative humidity above one hundred percent, as the time of cloud occurrence. Circles represent observations from radiosoundings.

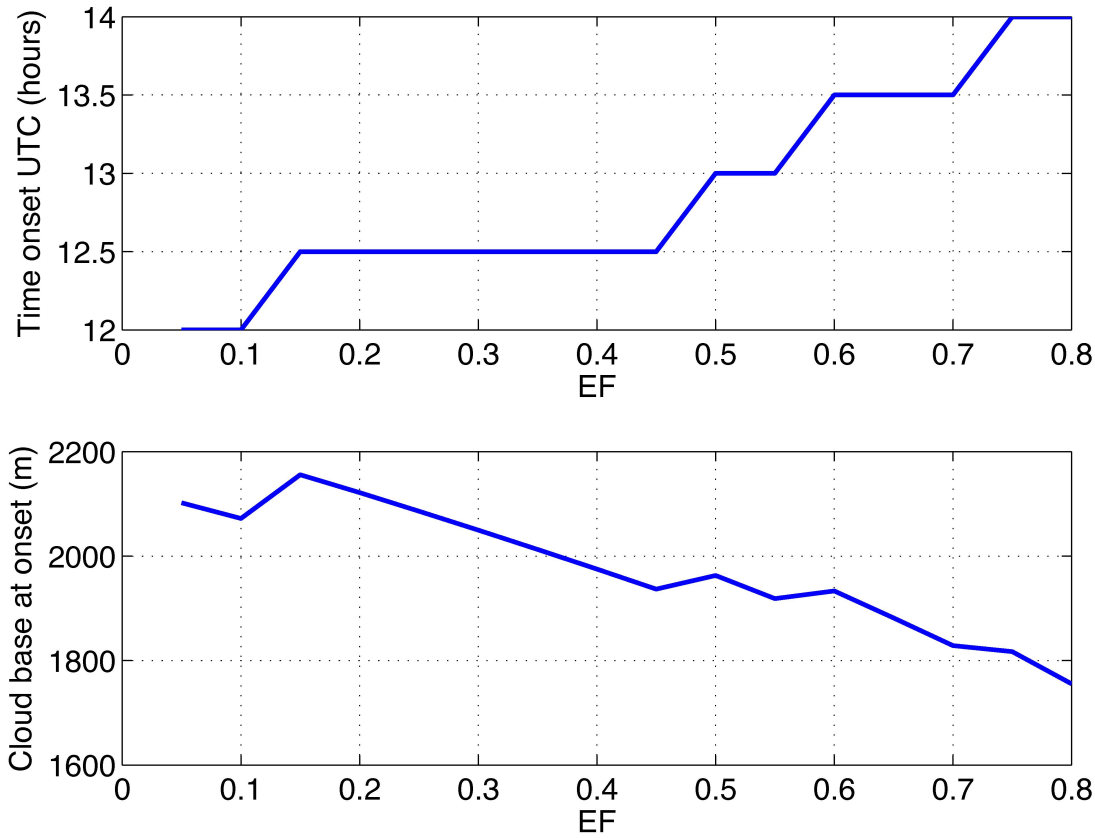

Figure 11: Cloud cover onset (top) and cloud base at onset (bottom) diagnosed with the mixed layer model for the AMMA dataset.

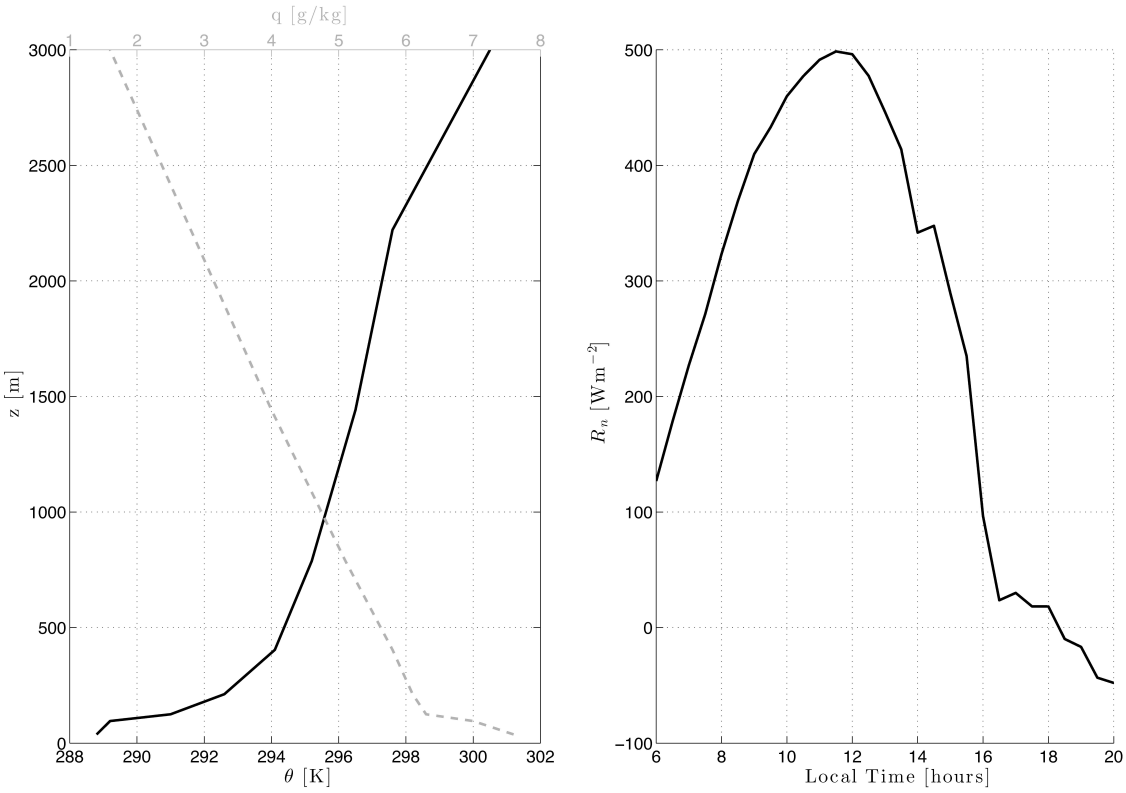

Figure 12: Potential temperature and specific humidity soundings at 6AM (UTC) (left) at the De Bilt site and diurnal course of net radiation at the Cabauw site (right).

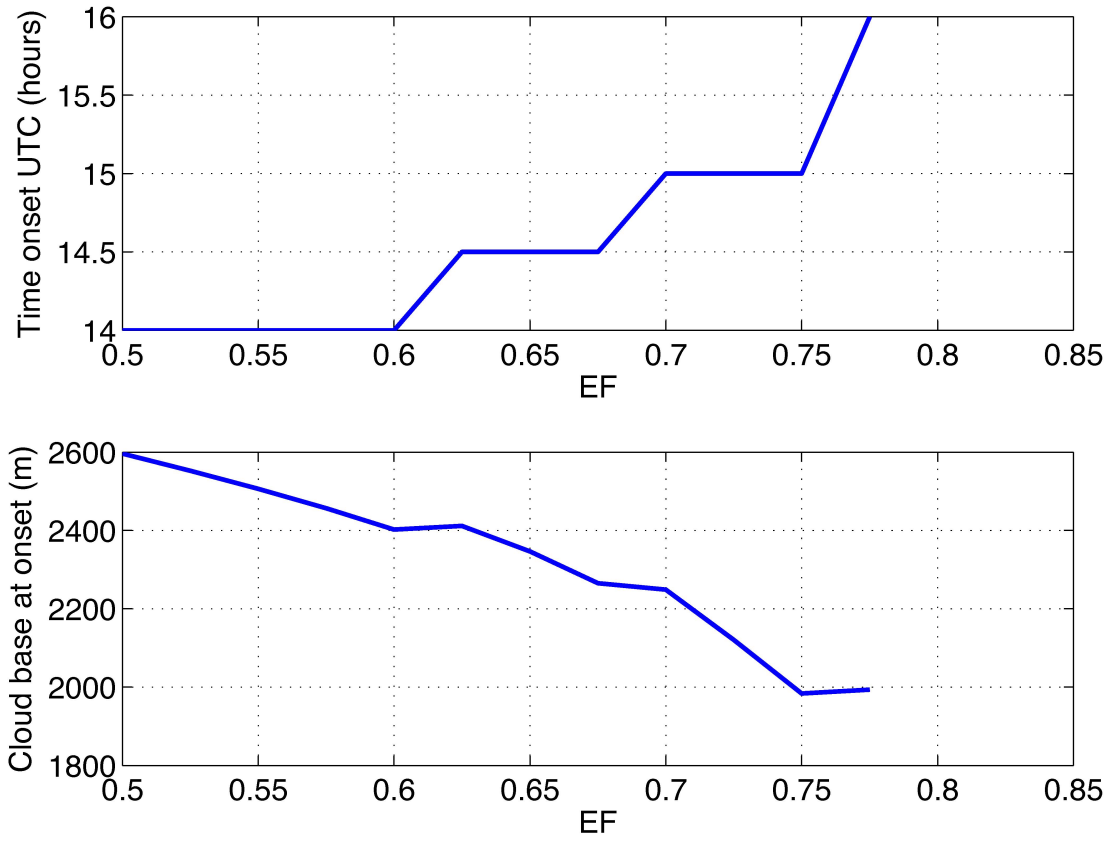

Figure 13: Same as Figure 11 but with the Cabauw land dataset. Observed cloud occurrence is between 1430 and 1500UTC.